Multi-parameter assessment of phytoplankton community composition from absorption, reflectance, and quantitative imaging

Sasha Kramer[1], Michael Brown[2], Collin Roesler[3], Nils Haëntjens[4]

[1]Interdepartmental Graduate Program in Marine Science, University of California Santa Barbara, Santa Barbara, California, USA // sasha.kramer@lifesci.ucsb.edu
[2]Department of Marine and Coastal Sciences, Rutgers University, New Brunswick, New Jersey, USA
[3]Department of Earth and Oceanographic Science, Bowdoin College, Brunswick, Maine, USA
[4]School of Marine Science, University of Maine, Orono, Maine, USA

Introduction and Background

Phytoplankton are microscopic photosynthesizers that are ubiquitous in the sunlit ocean; they form the base of the marine food web and are essential for oxygen production and carbon export from the surface to depth (Field et al. 1998). All phytoplankton contain pigments used for both photosynthesis and photoprotection. The composition of phytoplankton pigments differs between phytoplankton groups, making pigments useful chemotaxonomic markers for determining phytoplankton community structure (Jeffrey et al. 2011). Some pigments are associated with a specific taxonomic group: for instance, peridinin is a pigment that is found in dinoflagellates (although not all dinoflagellates contain peridinin). Other pigments, such as monovinyl chlorophyll-*a*, are found across the phytoplankton community in nearly all species of phytoplankton.

The composition and concentration of these pigments directly affects the shape and magnitude of the phytoplankton absorption coefficient; phytoplankton absorption can thus be used as a proxy for taxonomy. Changes in the shape of the phytoplankton absorption spectrum are driven to first order by concentration and composition of the pigments, but there is also second order variability due to pigment packaging and photoacclimation within the cell (Ciotti et al. 2002; Bricaud et al. 2004; Johnsen and Sakshaug 1996; MacIntyre et al. 2002). As reflectance is a function of absorption and scattering, the magnitude and shape of the phytoplankton absorption spectrum affects the magnitude and shape of the remote sensing reflectance spectrum (Roesler et al. 1989). In theory, the measured reflectance spectrum (or the difference between a measured and modeled reflectance spectrum using either measured or modeled phytoplankton absorption spectra) can then indicate phytoplankton community composition due to spectral anomalies associated with the presence and concentration of specific phytoplankton pigments.

While these optical and pigment-based proxies are used to determine phytoplankton taxonomy, the gold standard for assessing phytoplankton community composition is through cell quantification with microscopy and imaging. Microscopy is time consuming and can be less quantitative than methods like cell imaging, which allow for multiple attempts at taxonomic classification and validation after the original sample is processed (Olson and Sosik 2007). Ultimately, these methods all aim to describe the phytoplankton community for more than just the inherent value of understanding the taxonomic diversity of phytoplankton in the surface ocean. The chosen method of describing the phytoplankton community needs to also reflect the purpose of characterizing the community, whether for modeling purposes that broadly group phytoplankton taxa for their functional role in nutrient cycling and carbon export, for targeted identification of harmful algal bloom species to protect humans and fisheries from toxins, or otherwise.

With these various goals for taxonomic identification in mind, we here perform a multi-parameter assessment of phytoplankton taxonomy in a tidally variable coastal Maine estuary. Our optical data include phytoplankton absorption spectra and extracted pigment absorption spectra. We use measured remote sensing reflectance and an inversion model to compare the measured and

modeled phytoplankton absorption and remote sensing reflectance spectra. We confirm our results with direct assessment of phytoplankton community composition from quantitative imaging via the Imaging FlowCytobot. Across these four methods of taxonomic identification, our results show coherence between the optical proxies and the quantitative imaging data: a significant community of dinoflagellates emerges, indicated both by cell counts and spectral features in the optical data.

Approach

To characterize the phytoplankton community, we broadly used three approaches: absorption (by phytoplankton and by extracted phytoplankton pigments), radiometry, and quantitative imaging. All sampling took place on the R/V *Ira C.* in the Damariscotta River Estuary (DRE) on July 25 (day 1) and 26 (day 2), 2017. This site is in the Gulf of Maine (Fig. 1A), midcoast (Fig. 1B) and inland, midway between the Damariscotta River and Atlantic Ocean (Fig. 1C). Radiometry measurements were taken from the ship. Discrete water samples were collected at three depths (1 m., 5 m., and 12 m.) from the same station for use in the absorption and quantitative imaging methods.

1. Absorption

Discrete absorption spectra

Total particulate absorption coefficients (a_p) were determined spectrophotometrically by the Quantitative Filter Technique on discrete samples. Two 1-liter replicate water samples were collected from each depth at each station and particles from these water samples were filtered onto Whatman GF/F glass fiber filters. These filters were analyzed immediately on a Cary 300 dual beam spectrophotometer with an integrating sphere attachment. A hydrated blank filter was used in the reference beam. Absorption by phytoplankton (a_{ph}) and non-algal particles (a_{NAP}) were separated following the method of Kishino et al. (1985) by extracting the pigments with methanol and re-scanning the sample filter. Each filter was twice rotated 90 degrees and re-scanned, giving three replicate spectra for the total particulate absorption measurement and three for the non-algal particle measurement on each of the replicate water samples. The pathlength amplification factor of Stramski et al. (2015) was applied to all spectra to correct for effects of the filter.

Phytoplankton pigment absorption spectra

Total pigment absorption (a_{pig}) was measured on extracted phytoplankton pigments in solvent. Two 1-liter replicate water samples were collected from each depth at each station and filtered onto Whatman GF/F glass fiber filters. The pigments from each filter were extracted in 10 mL of 90% ethanol for 24 hours at below-freezing temperatures. The ethanol and extracted pigments solution was then centrifuged to remove any residual pieces of filter and the extract in solution was poured into 5 cm glass cuvettes for analysis on a Cary 50 single beam UV-vis spectrophotometer. 10 mL of pure 90% ethanol was used as a blank. The a_{pig} spectra were then decomposed into individual Gaussian peak pigment absorption spectra following the approach of Thrane et al. (2015). This method sums the pigment-specific absorption spectra by non-negative least squares multiple linear regression to reconstruct measured pigment absorption spectra. We used only pigments that overlap with coastal pelagic phytoplankton: chlorophyll-*a*, chlorophyll b, chlorophyll c_1, chlorophyll c_2, phaeophytin a, phaeophytin b, β-carotene, alloxathin, diadinoxanthin, diatoxanthin, dinoxanthin, fucoxanthin, lutein, neoxanthin, peridinin, violaxanthin, zeaxanthin, and phaeophorbide. We also digitized spectra for pure chlorophyll c_3 (Jeffrey and Wright 1987), 19'-butanoyloxyfucoxanthin (Jeffrey 1997), and 19'-hexanoyloxyfucoxanthin (Jeffrey 1997) in solvent. Pigment concentration was calculated from the magnitude of the deconstructed specific pigment absorption spectra and the specific absorption coefficients for each pigment (Jeffrey et al. 2011).

2. Radiometry

Remote sensing reflectance spectra

Measurements of hyperspectral remote-sensing reflectance (R_{rs}) were made using a hyperspectral Satlantic Surface Acquisition System (SAS) between 11 am and noon local time. The SAS consisted of three radiometers (one irradiance sensor and two radiance sensors). The irradiance radiometer was mounted on top of the vessel, and measured downwelling irradiance (E_d). The radiance radiometers were mounted on the stern of the vessel, oriented 135° from the solar azimuth and 40° from the nadir and zenith, and measured surface irradiance (L_t) and sky irradiance (L_i), respectively (Mobley et al. 1999; Mueller et al. 2003). During post-processing, the median E_d, L_t, and L_i over the sampling period of each cast was calculated to determine a representative spectrum, and the standard deviation of these values over the sampling period were calculated to determine variability. To remove the effects of white caps and sun glint, only the lowest 10% of the L_t spectra, assessed at 550 nm, were considered (Mueller et al. 2003). Next, R_{rs} was determined according to:

$$R_{rs} = (L_t - \rho * L_i)/E_d$$

where ρ is the surface reflectance factor, which was determined separately for each cast according to Mobley et al. (1999). The R_{rs} spectra were then linearly interpolated to every 3 nm, from 350 to 800 nm. To distinguish the observed R_{rs} from the modeled R_{rs}, we refer to this measurement as $R_{rs,obs}$.

Inversion modeling of inherent and apparent optical properties

The semi-analytical inversion model of Roesler and Perry (1995) was used to invert $R_{rs,obs}$ (from 440 to 749 nm) to derive the underlying inherent optical properties (IOPs), including a_{ph}. The inversion model solves the following equation:

$$R_{rs} \propto b_b/(a + b_b)$$

where the IOPs are separated, specifically absorption (a, which is the sum of a_{water}, a_{ph}, and a_{NAP}) and backscattering (b_b, which is the sum of b_{bw} and b_{bp}) spectra, and can be represented as the product of their spectral shape and magnitude. Using the derived IOPs from the inversion equation, we then forward modeled R_{rs}. To distinguish modeled R_{rs} from measured R_{rs}, we refer to this term as $R_{rs,mod}$. The difference spectrum between measured and modeled R_{rs} ($R_{rs,diff}$) gives information in $R_{rs,obs}$ not accounted for by the inversion model. Prior to calculating $R_{rs,diff}$, a 7 nm moving average was applied to $R_{rs,obs}$ and $R_{rs,mod}$ to smooth the spectra.

3. Quantitative imaging with the Imaging FlowCytobot

To validate the results of the optical measurements and modeling, we characterized the phytoplankton community using imaging-in-flow cytometry with the Imaging FlowCytobot (IFCB; Olson and Sosik 2007) using the fluorescence trigger to image fluorescing particles. The IFCB counts and images large nano- and microplankton (>8 μm). Cell taxonomy and biovolume for each cell were determined using image analysis according to Moberg and Sosik (2012); images were further classified, validated, and exported using EcoTaxa software (Picheral et al. 2017). The images for this project can be found at http://ecotaxa.obs-vlfr.fr/prj/799. During post-processing and analysis, all non-living particles (detritus, plastic, feces, bubbles, etc.) were discarded and are not included in total biovolume calculations.

Results

Coherence of results across days, depths, and methods

With a few exceptions, we see a remarkable consistency in these results across the two sampling days, the three sampling depths, and the different methods. Nearly all measured a_{ph}

spectra match both each other and the retrieved a_{ph} spectra from the inversion modeling (Figs. 2 and 5). The a_{pig} spectra (Fig. 3) show similar spectral features to each other, to the a_{ph} spectra, and to the $R_{rs,diff}$ spectra (Fig. 4), specifically at 475 nm, which is the absorption peak for peridinin (a marker pigment in dinoflagellates). Finally, the quantitative imaging results confirm the presence of a dinoflagellate community in addition to high numbers of diatoms and nanoplankton (Fig. 6).

1. Absorption

The a_{ph} spectra show similar spectral features across the two days of sampling and the three depths (Fig. 2A). The pronounced absorption peak in the red wavelengths indicates high chlorophyll-*a* concentration; similarly, there is high absorption by chlorophyll and other phytoplankton pigments across the blue wavelengths and a similar shape of the absorption spectrum in the blue, suggesting the presence of a similar suite of phytoplankton pigments between the two days of sampling. The only spectrum with a different spectral shape is the spectrum from day 2 at 5 meters, which has anomalously low magnitude absorption in the blue. The a_{pig} spectra are also quite similar between sampling days and depths. Following the decomposition of a_{pig} spectra into pigment-specific absorption spectra (Fig. 3A), the pigments with the highest magnitude absorption across all samples are monovinyl chlorophyll-*a*, monovinyl chlorophyll b, and peridinin (Fig. 3B). Finally, both the spectral shape and the magnitude of the modeled a_{ph} spectra for days 1 and 2 match the measured phytoplankton absorption spectra measured by the QFT (Figs. 5A and 5B).

2. Radiometry

The measured remote sensing reflectance spectra, $R_{rs,obs}$, from day 2 are much higher in magnitude than the spectra from day 1 (Fig. 4A). Once the spectra have been normalized to the area under the curve, the spectral shapes of the two $R_{rs,obs}$ spectra, however, are quite similar (Fig. 4B) in the green and red wavelengths, but different in the blue wavelengths where the day 1 spectra are much flatter and the day 2 spectra are much steeper. As part of the inversion modeling process, we also conducted a sensitivity analysis on the Roesler and Perry (1995) model. The results of the sensitivity analysis (data not shown) confirmed that the value of the slope of colored dissolved organic matter (CDOM) absorption strongly affects the accuracy of the a_{ph} retrieval. However, for the DRE, the default CDOM slope (0.0145) determined by Roesler et al. (1989) and used in Roesler and Perry (1995) is appropriate (compared to field measurements of CDOM and non-algal particle absorption from this same field study, data not shown).

The forward modeled remote sensing reflectance spectrum minus the measured reflectance spectrum results in the difference spectrum ($R_{rs,diff}$, Fig. 5C), which shows spectral features at wavelengths dominated by phytoplankton absorption (440-500 nm in the blue and 590-710 in the red). Specifically, there is a strong feature at 475 nm, which is the wavelength of peak absorption for peridinin, which is a marker pigment found only in dinoflagellates.

3. Quantitative imaging with the Imaging FlowCytobot

Our quantitative imaging with the IFCB resulted in a total of 97,245 images from 12 samples (replicate samples run at each depth for each day of sampling). After removing non-living particles from the total image count, there were between 5,000 and 12,000 cells per sample (1,900-3,700 cells per milliliter of seawater sampled). Due to the high concentration of cells in our samples (5-17k cells/sample), our average volume sampled was lower than the 5 mL standard to the IFCB. However, this lower sample volume is considered to be representative of the sample, as the IFCB imaged cells consistently throughout the sampling time (Heidi Sosik, *pers. comm.*).

All images were classified to taxonomic group or species level by an automated classifier and then validated individually. There were 37 distinct groups or species of living plankton that were identified in this dataset. These groups can be broadly categorized into ten taxonomic groups (Fig. 6): centric and pennate diatoms (both individual cells and chains of cells), dinoflagellates, ciliates, nanoplankton (cells between 2-10 μm too small to be identified with further taxonomic specificity), cryptophytes, prymnesiophytes, clumps (distinctive cells with detritus), multiples (more than one cell per image), and other living cells (all other fluorescing cells of all sizes and morphologies). The distribution of cells by biovolume was relatively similar between day 1 and day 2 with a higher proportion (~15-20%) of clumps and detritus on day 2 than day 1 and more nano-sized phytoplankton (~10-15%) on day 1 than day 2. On both days, centric and pennate diatoms and a number of dinoflagellate species were present and accounted for large proportions (25-45%) of the total biovolume of cells.

Discussion

These disparate methods show quite similar results across the two sampling days and the three sampling depths. Here, we will describe sources of variability between methods and challenges associated with each method. First, the absorption data were similar across measured and modeled parameters, with the exception of one spectrum (Fig. 2A). As the a_{ph} spectrum is calculated as the difference between the measured particle absorption and non-algal particle absorption spectra, the one anomalous spectrum is an example of oversaturation on the filter pad. The total particulate (a_p) absorption spectrum suggests a lower concentration of non-algal particles, but following the methanol extraction and removal of pigmented particles from the filter pad, the non-algal particle absorption spectrum reveals a higher density of non-algal particles. This result then gives an unrealistic shape and magnitude for the phytoplankton absorption spectrum, as shown here.

The spectral decomposition of a_{pig} resulted in high concentrations of monovinyl chlorophyll *a* and b as well as peridinin; the presence and concentation of these pigments can be used to infer phytoplankton community structure. All phytoplankton species contain monovinyl chlorophyll-*a* except *Prochlorococcus* sp., which contains divinyl chlorophyll *a* (Chisholm et al., 1992). Monovinyl chlorophyll b is found in pico- to nano-sized phytoplankton, specifically those with a green algal lineage such as chlorophytes (Falkowski et al. 2004; Jeffrey et al. 2011). Peridinin is a distinctive marker pigment found in many species of dinoflagellates. While pigments are not always definitive markers for phytoplankton taxonomy, all of these taxonomic groups were identified as significant contributors to overall biovolume in the IFCB results (Fig. 6). It was outside of the scope and budget of this project to compare the a_{pig} concentrations to another method of measuring phytoplankton pigments, specifically High Performance Liquid Chromatography (HPLC). However, the methods described here were replicated during a research cruise in the Santa Barbara Channel, California in December 2017 and compared to HPLC analysis conducted at the NASA Goddard Space Flight Center. The results showed a positive linear relationship between all pigments measured by HPLC and by the a_{pig} spectra, with the a_{pig} approach underestimating the pigment concentration (i.e., for total chlorophyll-*a*, Fig. 3C).

Finally, the remote sensing reflectance spectra had surprisingly good correspondence with the measured absorption and phytoplankton community composition data, given the high concentrations of CDOM and non-algal particles in the DRE. The higher magnitude of reflectance on day 2 indicates a larger contribution of backscattering relative to absorption on day 2 compared to day 1. The phytoplankton absorption spectra from day 1 and day 2 are relatively similar in magnitude and shape (Fig. 2A), but the particle absorption spectra show a much higher contribution

relative of non-algal particle absorption on day 2 (data not shown), suggesting that there would also be more scattering by non-algal particles on day 2 and thus a higher magnitude reflectance spectrum.

Finally, the IFCB allows us to describe dominant features in phytoplankton community structure, but also explore other noteworthy trends in the data that would not have been visible without the use of this instrument. For instance, we found a large community of "dirty" *Thalassiosira* sp. cells (a centric, chain-forming diatom; Fig. 6B, denoted with a red asterisk). These cells appear in all samples across all depths during our sampling; they are covered in detrital matter and are quite different from the crisp frustules that define most siliceous diatom cells. Similarly, we were able to image ciliates, which are not photosynthetic but heterotrophic or mixotrophic organisms, and otherwise would not have been distinct in the optical data. One weakness of using the IFCB is the limited size range of cells imaged by the instrument: only nano- and micro-sized phytoplankton communities, $\geq\cong 8$ μm, are described here due to the resolution of the instrument. We cannot quantify the picoplanktonic community or further describe the variability in small nano-sized cells.

Ultimately, across both optical and quantitative imaging methods, between sampling days, and over sampling depths, similar features emerge that suggest high phytoplankton biomass with the presence of a dinoflagellate community. These results are clearest from the IFCB data, where the number of cells and the proportion of dinoflagellates to total cell biovolume can be exactly enumerated. However, the spectral data also show a high concentration of peridinin, which is a pigment found only in dinoflagellate species, as well as features at 475 nm which is the absorption peak of peridinin.

Conclusions

There are many existing methods of phytoplankton taxonomic identification, both in situ and from remote sensing; as we have shown here, some of these approaches, such as quantitative imaging, allow for a higher degree of taxonomic specificity than optical proxies in that they can exactly enumerate cells and visually characterize unusual features within the phytoplankton community. However, these methods are also more expensive and sample relatively less of the ocean at a time (milliliters of seawater compared to liters or square surface meters). Often, the decision to use one method over another is motivated by budget, time, or space concerns. The choice of method also depends on the targeted phytoplankton taxonomic group or species. For instance, this region of the Gulf of Maine experiences harmful algal blooms: here we show that it is possible to identify the presence of a dinoflagellate community across a variety of hyperspectral optical methods, but only the IFCB images could show the species-level composition of that dinoflagellate community to determine that the cells were not a bloom of a harmful or toxic species (such as *Alexandrium fundyense*).

Ideally, higher taxonomic resolution of phytoplankton groups in the surface ocean will be possible with the development of hyperspectral satellite sensors (such as the NASA Plankton Aerosol Cloud and ocean Ecosystem [PACE] sensor, https://pace.oceansciences.org). If we had only measured hyperspectral remote sensing reflectance here (Fig. 4) and performed an inversion analysis (Fig. 5), we would have seen spectral features at the same wavelength as the peak of peridinin absorption (~475 nm), which could allow us to speculate about the presence of a dinoflagellate community even without further in situ measurements specific to the phytoplankton community. There are many caveats and challenges to using these optical and pigment-based methods to describe the number and composition of phytoplankton cells in the surface ocean. However, the results presented here suggest that there can be coherence between these disparate methods that allows for broad conclusions about the presence of specific taxonomic groups within the overall phytoplankton community from just one data source, such as remote sensing reflectance.

Acknowledgements
Thank you to Captain Robbie Downs of the *Ira C.* for support in collecting samples. SK and MB conducted this project during the Ocean Optics course; we wish to especially thank NH for his support as our TA and CR for her guidance and encouragement as our professor. We are grateful for advice and help on this project from Emmanuel Boss and Curt Mobley. Thank you to Ali Chase and Heidi Sosik for image analysis support and tips for the IFCB. Kelsey Bisson provided helpful edits that greatly improved an earlier version of this work.

Figures

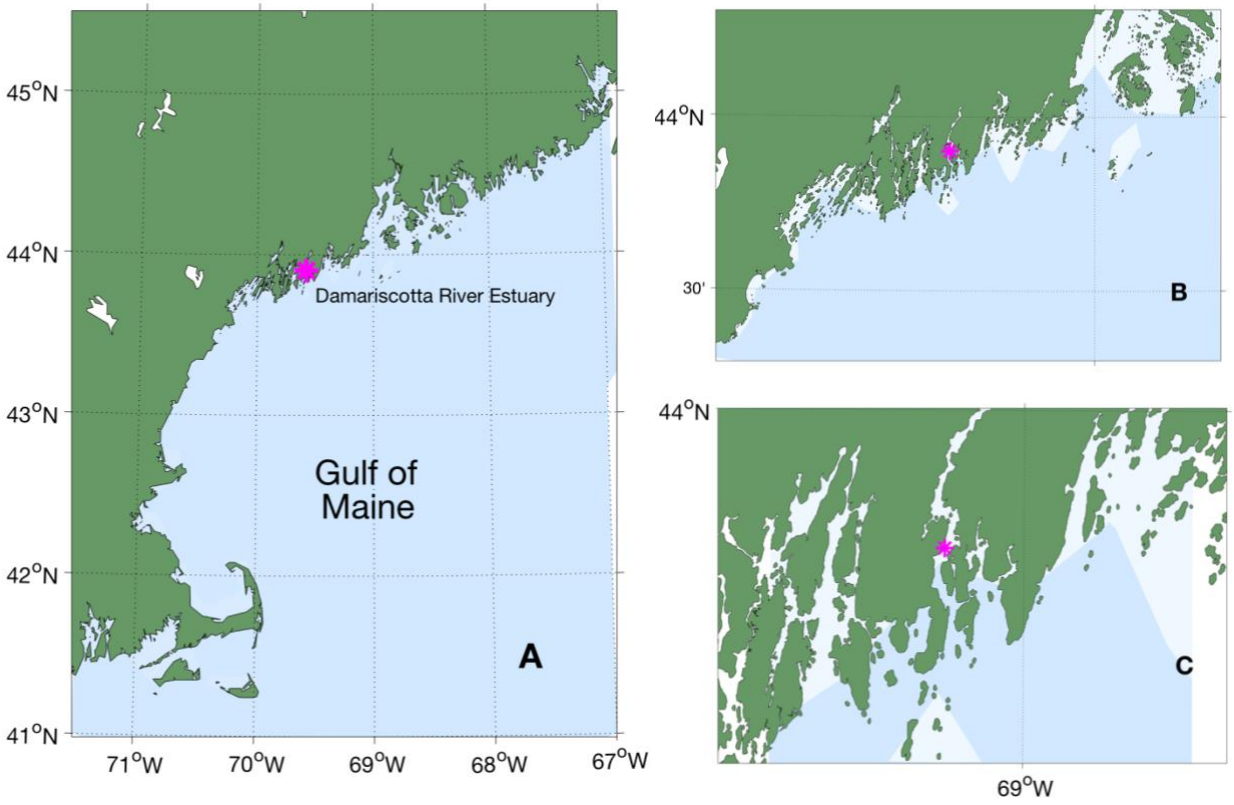

Figure 1. Location of sample collection in the Damariscotta River Estuary, Maine, USA.

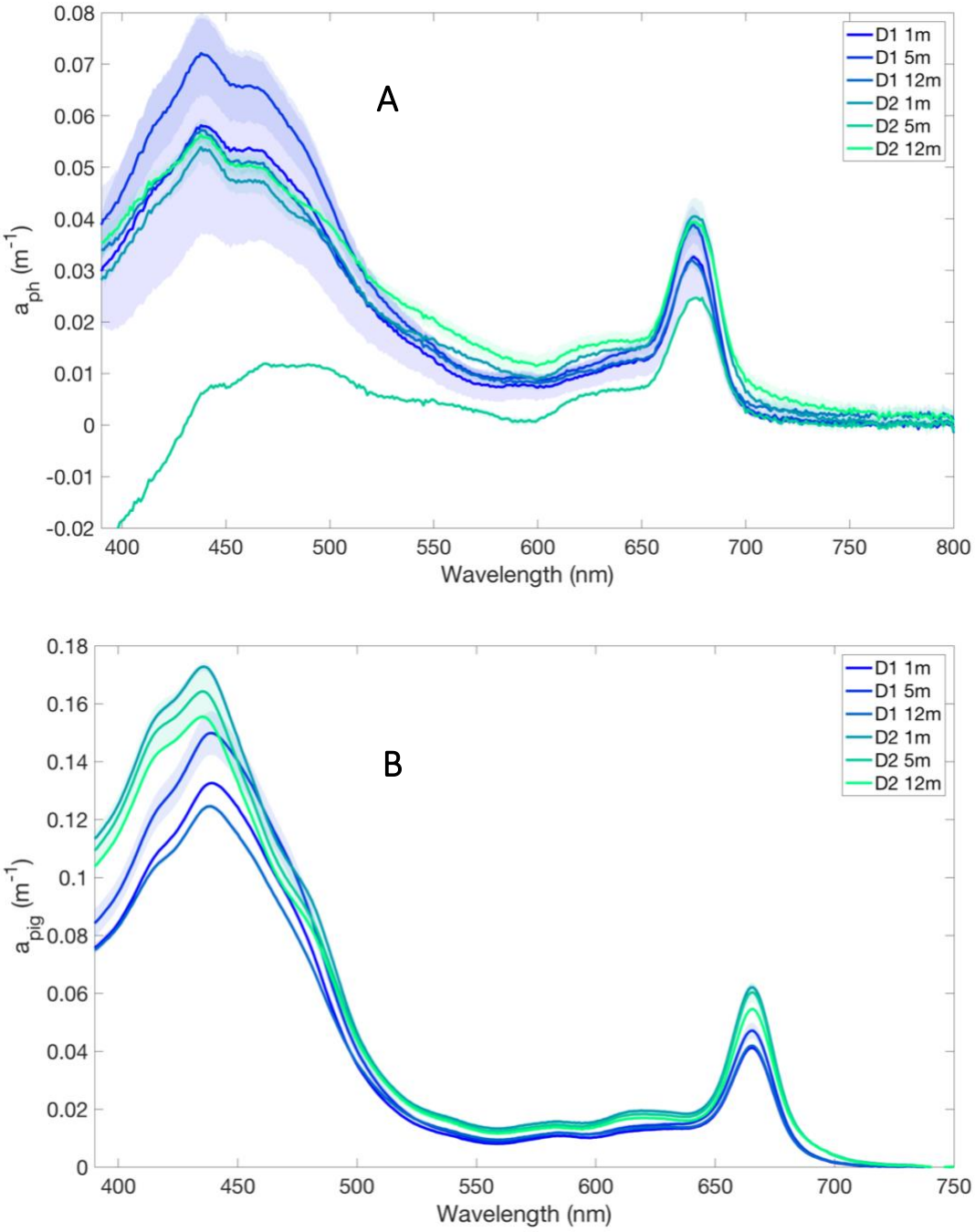

Figure 2. (A) Phytoplankton absorption spectra and (B) pigment absorption spectra at all depths for day 1 and day 2.

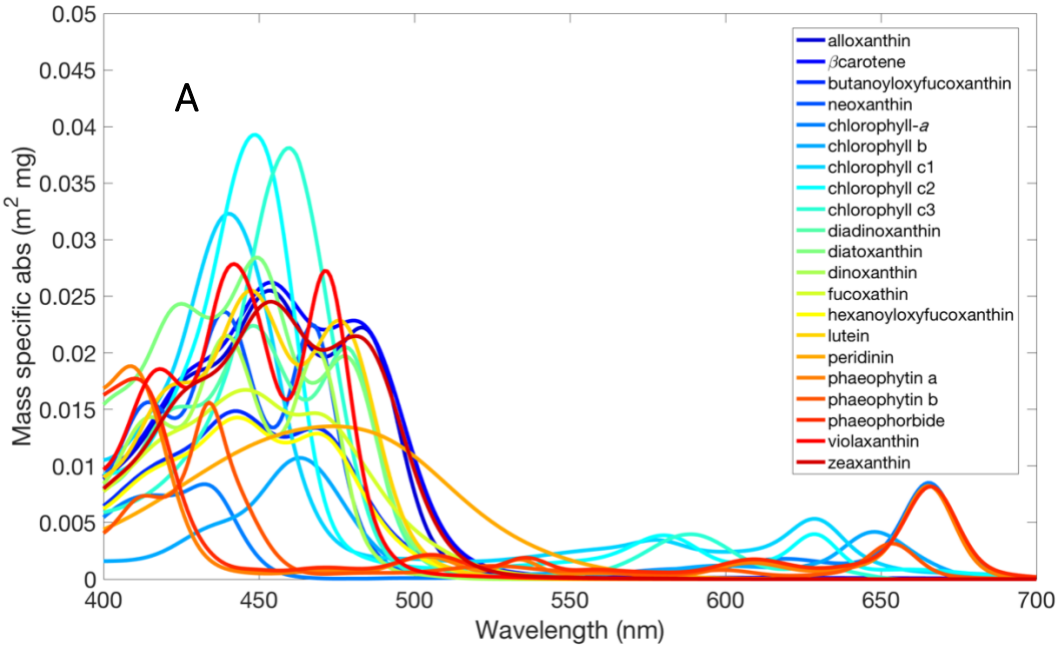
A
Mass specific abs (m^2 mg)
Wavelength (nm)
alloxanthin
βcarotene
butanoyloxyfucoxanthin
neoxanthin
chlorophyll-a
chlorophyll b
chlorophyll c1
chlorophyll c2
chlorophyll c3
diadinoxanthin
diatoxanthin
dinoxanthin
fucoxathin
hexanoyloxyfucoxanthin
lutein
peridinin
phaeophytin a
phaeophytin b
phaeophorbide
violaxanthin
zeaxanthin

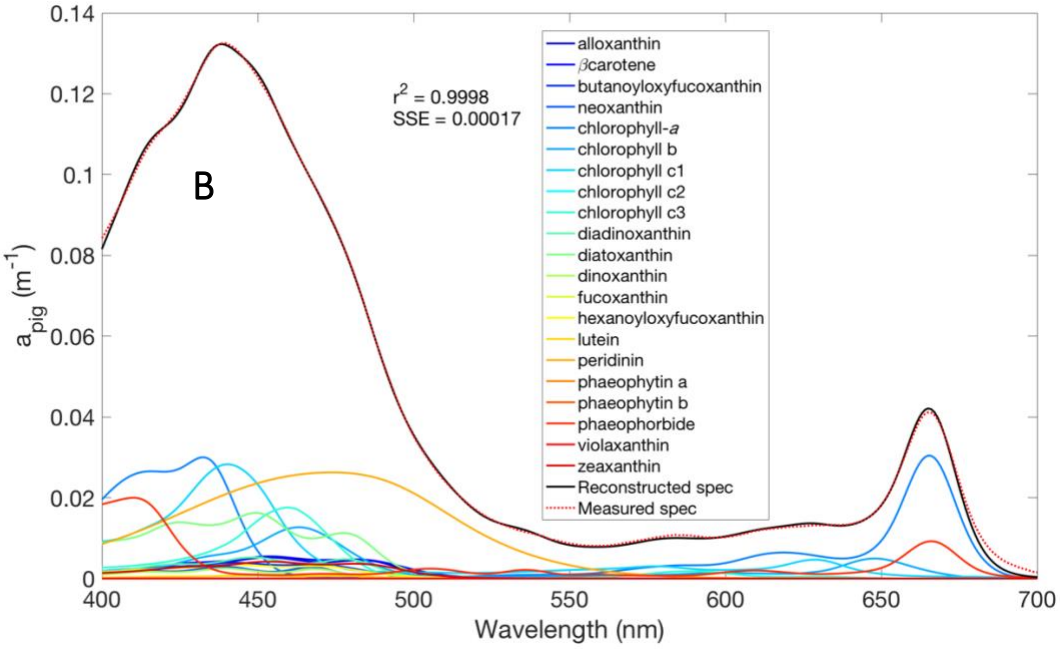
B
r^2 = 0.9998
SSE = 0.00017
a$_{pig}$ (m^{-1})
Wavelength (nm)
alloxanthin
βcarotene
butanoyloxyfucoxanthin
neoxanthin
chlorophyll-a
chlorophyll b
chlorophyll c1
chlorophyll c2
chlorophyll c3
diadinoxanthin
diatoxanthin
dinoxanthin
fucoxanthin
hexanoyloxyfucoxanthin
lutein
peridinin
phaeophytin a
phaeophytin b
phaeophorbide
violaxanthin
zeaxanthin
Reconstructed spec
Measured spec

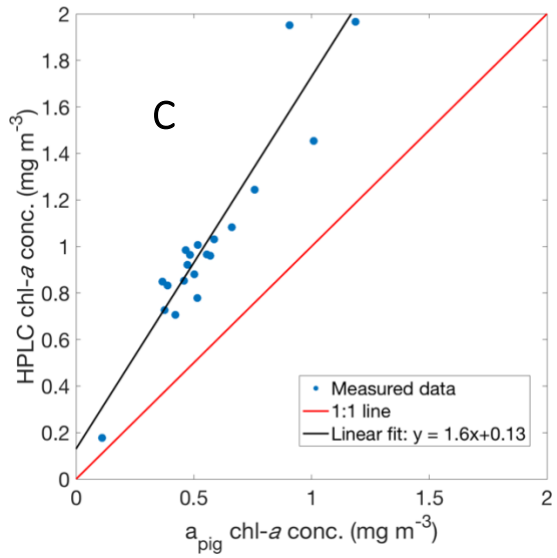

Figure 3. Pigment absorption spectra results. (A) Mass specific absorption of each pigment used in this analysis. (B) Reconstruction of the pigment absorption spectra using the Thrane et al. (2015) approach for day 1, 1 meter depth. (C) Total chlorophyll-*a* concentration determined by pigment absorption vs. total chlorophyll-*a* measured from HPLC (data from Santa Barbara Channel, CA).

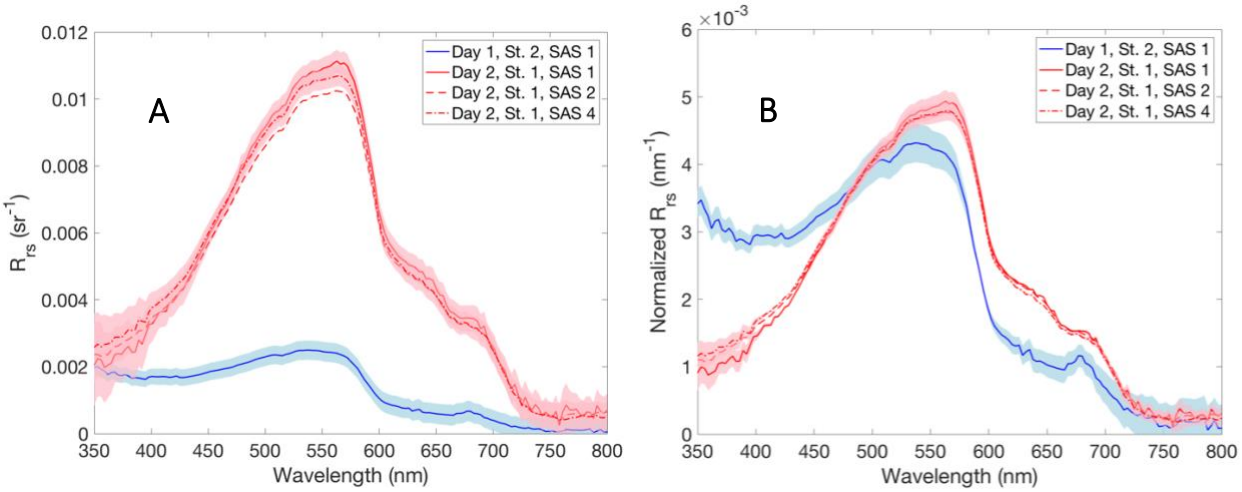

Figure 4. HyperSAS measurements for day 1 (blue) and day 2 (red); shaded region shows ± one standard deviation of the mean. (A) Actual measured value of remote sensing reflectance. (B) Remote sensing reflectance normalized to the area under the curve.

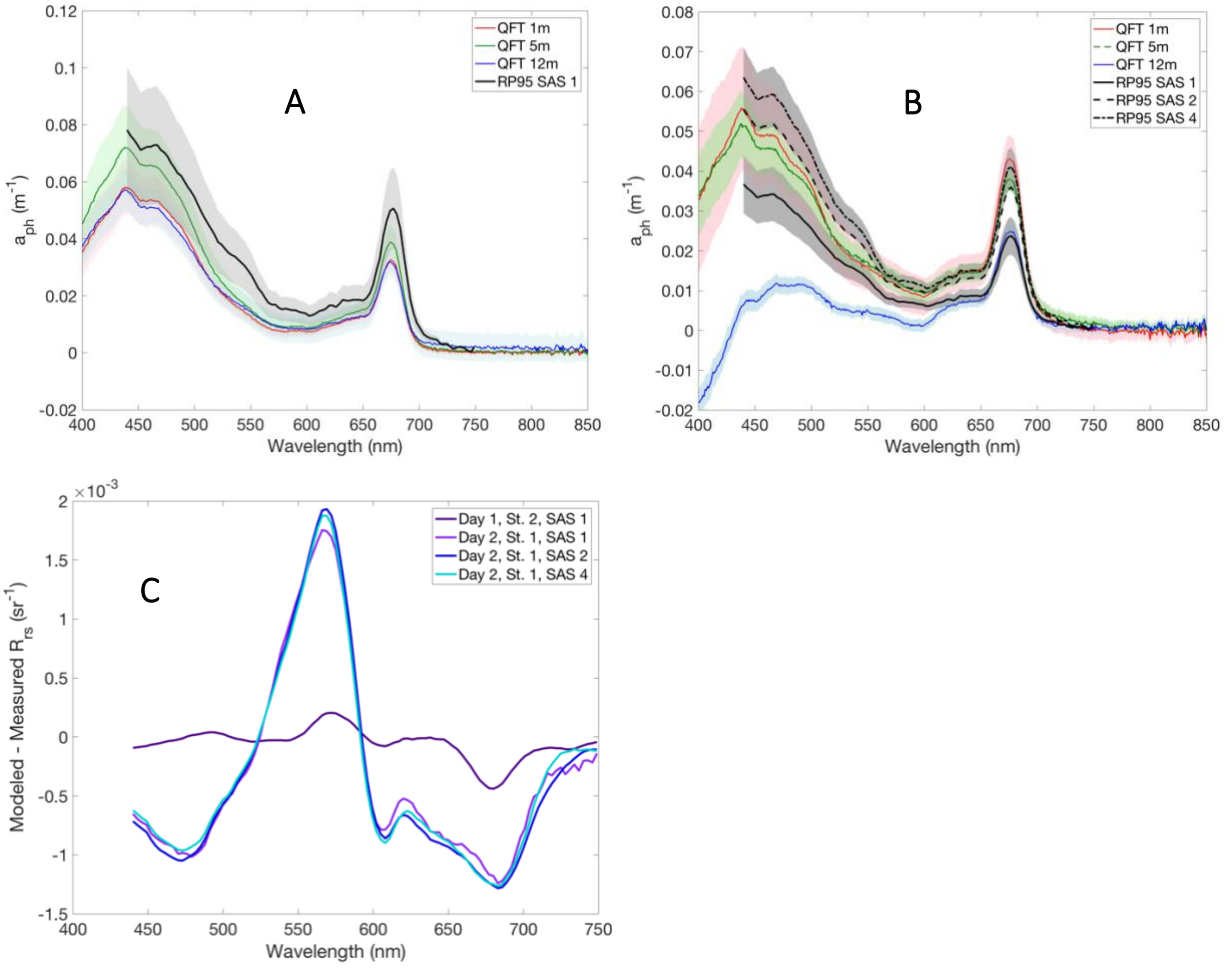

Figure 5. Roesler and Perry (1995) remote sensing reflectance inversion model a_{ph} results (black) vs. measured data at 1 meter (red), 5 meters (green), and 12 meters (blue) for (A) day 1 and (B) day 2. (C) Modeled minus measured R_{rs} spectra for day 1 (dark purple) and day 2 (light purple, blue, turquoise).

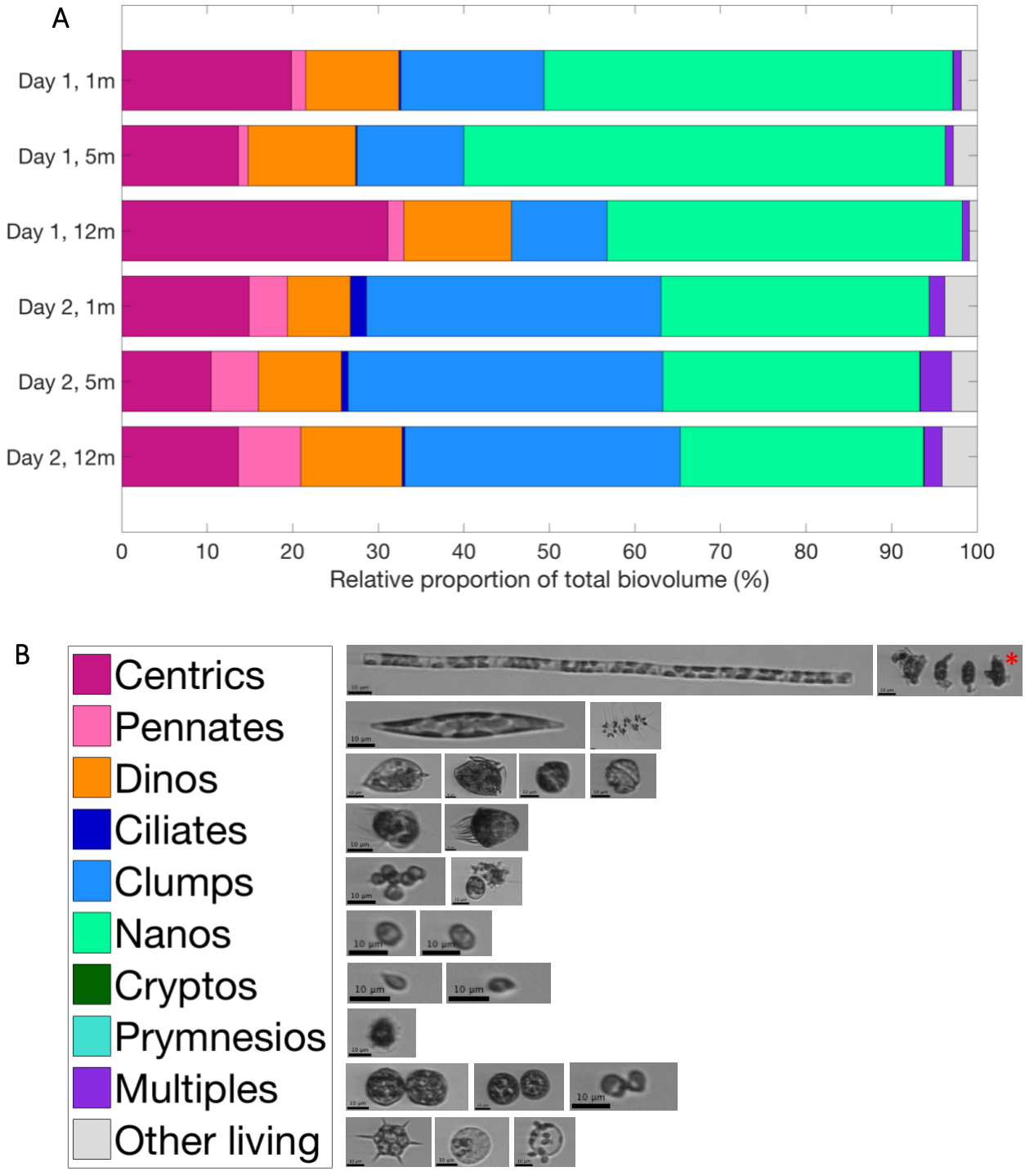

Figure 6. (A) Relative proportion of each taxonomic group (centric diatoms, pennate diatoms, dinoflagellates, ciliates, clumps, nanoplankton, cryptophytes, prymnesiophytes, multiple cells, and other living cells) to total biovolume ($\mu m^3/mL$) of cells measured by the Imaging FlowCytobot for each sampling day and at each sample depth. (B) Examples of cells from each major taxonomic group imaged by the IFCB for this project.

References

Bricaud, A., Claustre, H., Ras, J. and K. Oubelkheir, K., 2004. Natural variability of phytoplanktonic absorption in oceanic waters: Influence of the size structure of algal populations. *J. Geophys. Res. 109*, 1-12. doi:10.1029/2004JC002419.

Chisholm, S.W., Frankel, S.L., Goericke, R., Olson, R.J., Palenik, B., Waterbury, J.B., West-Johnsrud, L., and Zettler, E.R., 1992. *Prochlorococcus marinus* nov. gen. nov. sp.: an oxyphototrophic marine prokaryote containing divinyl chlorophyll a and b. *Arch. Microbiol. 157*, 297-300. doi:10.1007/BF00245165.

Ciotti, Á.M., Lewis, M.R. and Cullen, J.J., 2002. Assessment of the relationships between dominant cell size in natural phytoplankton communities and the spectral shape of the absorption coefficient. *Limnol. Oceanogr.* 47(2), 404-417. doi:10.4319/lo.2002.47.2.0404.

Falkowski, P.G., Katz, M.E., Knoll, A.H., Quigg, A., Raven, J.A., Schofield, O. and Taylor, F.J.R., 2004. The evolution of modern eukaryotic phytoplankton. *Science* 305, 354-360. doi:10.1126/science.1095964.

Field, C.B., Behrenfeld, M.J., Randerson, J.T., and Falkowski, P., 1998. Primary production of the biosphere: Integrating terrestrial and oceanic components. *Science* 281, 237-240, doi:10.1126/science.281.5374.237.

Jeffrey, S.W. and Wright, S.W., 1987. A new spectrally distinct component in preparations of chlorophyll c from the micro-alga *Emiliania huxleyi* (Prymnesiophyceae). *Biochim. Biophys. Acta* 894, 180–188. doi:10.1016/0005-2728(87)90188-5.

Jeffrey, S.W., 1997. Application of pigment methods to oceanography. In: Jeffrey, S.W., Mantoura, R.F.C., Wright, S.W. (eds.), Phytoplankton pigments in oceanography: guidelines to modern methods. *UNESCO Monogr. Oceanogr. Methodol.,* Vol 10, UNESCO Publishing, Paris, 127–165.

Jeffrey, S.W., Wright, S.W., and Zapata, M., 2011. Microalgal classes and their signature pigments, in *Phytoplankton Pigments: Characterization, Chemotaxonomy, and Application in Oceanography*, edited by S. Roy, C. A. Llewellyn, E. S. Egeland and G. Johnsen, pp. 3-77, Cambridge University Press, Cambridge, United Kingdom.

Jensen, A., and Sakshuag, E., 1973. Studies on the phytoplankton ecology of the Trondheimsfjord. II. Chloroplast pigments in relation to abundance and physiological state of the phytoplankton. *J. Exp. Mar. Biol. Ecol. 11*, 137-155. doi:10.1016/0022-0981(73)90052-X.

Kishino, M., Takahashi, M., Okami, N., Ichimura, S., 1985. Estimation of the spectral absorption coefficients of phytoplankton in the sea. *Bull. Mar. Sci.* 37 (2), 634–642.

MacIntyre, H.L., Kana, T.M., Anning, T., and Geider, R.J., 2002. Photoacclimation of photosynthesis irradiance response curves and photosynthetic pigments in microalgae and cyanobacteria. *J. Phycol. 38*, 17-38. doi: 10.1046/j.1529-8817.2002.00094.x.

Moberg, E.A., and Sosik, H.M., 2012. Distance maps to estimate cell volume from two-dimensional plankton images. *Limnol. Oceanogr. Meth.* 10, 278-288, doi:10.4319/lom.2012.10.278.

Mobley, C.D., 1999, Estimation of the remote-sensing reflectance from above-surface measurements. *Appl. Opt.* 38 (36), 7442–7455. doi:10.1364/AO.38.007442.

Mueller, J.L., Pietras, C., Hooker, S.B., Austin, R.W., Miller, M., Knobelspiesse, K.D., et al., 2003. Ocean optics protocols for satellite ocean color sensor validation: Revision 4. Instrument specifications, characterization and calibration. *NASA Tech. Memo.* vol. 2003-21621. Greenbelt, MD: National Aeronautics and Space Administration, Goddard Space Flight Center.

Olson, R.J., and Sosik, H.M., 2007. A submersible imaging-in-flow instrument to analyze nano- and microplankton: Imaging FlowCytobot. *Limnol. Oceanogr. Meth.* 5(6), 195-203, doi:10.4319/lom.2007.5.195.

Picheral M., Colin S., Irisson J.-O., 2017. EcoTaxa, a tool for the taxonomic classification of images. http://ecotaxa.obs-vlfr.fr.

Roesler, C.S. and Perry, M.J., 1995, In situ phytoplankton absorption, fluorescence emission, and particulate backscattering spectra determined from reflectance. *J. Geophys. Res.* 100, 13,279–13,294. doi:10.1029/95JC00455.

Roesler, C.S., Perry, M.J. and Carder, K.L., 1989. Modeling in situ phytoplankton absorption from total absorption spectra in productive inland marine waters. Limnol. Oceanogr., 34(8), 1510-1523. doi:10.4319/lo.1989.34.8.1510.

Stramski, D., Reynolds, R.A., Kaczmarek, S., Uitz, J., and Zheng, G., 2015, Correction of pathlength amplification in the filter-pad technique for measurements of particulate absorption coefficient in the visible spectral region. *Appl. Opt.* 54 (22), 6763–6782. doi:10.1364/AO.54.006763.

Thrane, J.E., Kyle, M., Striebel, M., Haande, S., Grung, M., Rohrlack, T., Andersen, T., 2015. Spectrophotometric analysis of pigments: A critical assessment of a high-throughput method for analysis of algal pigment mixtures by spectral deconvolution. *PLoS ONE* 10 (9), 1–24. doi:10.1371/journal.pone.0137645.